AGU100 ADVANCING EARTH AND SPACE SCIENCE

Geophysical Research Letters

RESEARCH LETTER
10.1029/2018GL081584

Key Points:
- We use CubeSat satellite imagery and machine learning to track sub-seasonal changes in surface water area for 85,358 Arctic-Boreal lakes
- We observe a broad-scale seasonal decline in lake area dominated by small (<10 m), previously unquantified, lake shoreline contractions
- The sum of these contractions reveals that lake-dense areas experience substantial water loss with implications for trace-gas emissions

Supporting Information:
- Supporting Information S1

Correspondence to:
S. W. Cooley,
sarah_cooley@brown.edu

Citation:
Cooley, S. W., Smith, L. C., Ryan, J. C., Pitcher, L. H., & Pavelsky, T. M. (2019). Arctic-Boreal lake dynamics revealed using CubeSat imagery. *Geophysical Research Letters*, *46*, 2111–2120. https://doi.org/10.1029/2018GL081584

Received 4 DEC 2018
Accepted 24 JAN 2019
Accepted article online 4 FEB 2019
Published online 19 FEB 2019

Arctic-Boreal Lake Dynamics Revealed Using CubeSat Imagery

Sarah W. Cooley[1,2], Laurence C. Smith[3], Jonathan C. Ryan[2], Lincoln H. Pitcher[3], and Tamlin M. Pavelsky[4]

[1]Department of Earth, Environmental and Planetary Sciences, Brown University, Providence, RI, USA, [2]Institute at Brown for the Environment and Society, Brown University, Providence, RI, USA, [3]Department of Geography, University of California, Los Angeles, CA, USA, [4]Department of Geological Sciences, University of North Carolina at Chapel Hill, Chapel Hill, NC, USA

Abstract Fine-scale, subseasonal fluctuations in Arctic-Boreal surface water reflect regional water balance and modulate trace gas emissions to the atmosphere but have eluded detection using traditional satellite remote sensing. We use high-resolution (~3–5 m), high-frequency CubeSat sensors to measure near-daily changes in lake surface area through an object-based tracking method that incorporates machine learning to overcome notable limitations of CubeSat imagery. From ~76,000 images we obtain >2.2 million individual observations of changing surface areas for 85,358 lakes in Northern Canada and Alaska between 1 May and 1 October 2017. We find broad-scale lake area declines across diverse climatic, hydrologic, and physiographic terrains. Localized exceptions reveal lowland flooding and aquatic vegetation phenology cycles. Cumulative small shoreline changes of abundant lakes on the Canadian Shield exceed total inundation variations of better-studied lowland environments, revealing a surprisingly dynamic landscape with respect to subseasonal variations in surface water extent and trace gas emissions.

Plain Language Summary Fluctuations in Arctic-Boreal lakes reflect climate change and regulate freshwater methane and CO_2 emissions. Observing these fine-scale changes has traditionally been difficult due to the coarse spatial and temporal resolution of available satellite imagery. Recently, however, the launch of hundreds of tiny satellites known as CubeSats has created new opportunities for monitoring lake area through providing daily imagery at 3-m resolution. Here we present a new method for tracking lake area changes using CubeSat imagery, which overcomes limitations that have, until now, prevented large-scale CubeSat analyses. Using this method, we track changes in lake area for ~85,000 lakes across Northern Canada and Alaska between May and October 2017. We observe a general seasonal decline in lake area across diverse terrains but identify localized exceptions caused by wetland flooding and the growth and decline of vegetation on the lake surface. Surprisingly, the greatest absolute lake area changes occur in upland, lake-dense terrains previously thought to be very stable. In these regions, small (<10 m) changes along lake margins cumulatively sum to large changes in total lake area that are largely undetectable from coarser-resolution satellites. This previously unquantified lake area variability suggests that models may underestimate greenhouse gas emissions in these regions.

1. Introduction

The Arctic-Boreal region contains the highest density of lakes on Earth (Lehner & Döll, 2004; Pekel et al., 2016; Verpoorter et al., 2014). Their areal extents fluctuate seasonally and interannually in response to regional water balance, fluvial inundation, and surface-groundwater interactions. Variability in lake extent is thus a useful indicator of diverse climatic and physiographic processes (Tranvik et al., 2009). Furthermore, because Arctic-Boreal lakes are net sources of CO_2 and CH_4 (Hastie et al., 2018), fluctuations in lake area impact freshwater trace gas emissions to the atmosphere (Bastviken et al., 2011; Raymond et al., 2013). Lake shoreline variability is especially important because shallow water, vegetation, and CO_2 supersaturation intensify trace gas emissions along seasonally inundated lake perimeters (Bastviken et al., 2004; Tranvik et al., 2009). Quantifying the subseasonal variability of Arctic-Boreal lake areas is therefore critical for improving estimates of trace gas flux (Kirschke et al., 2013; Stackpoole et al., 2017) and understanding the hydrological sensitivity of lakes to geological substrate, water balance, fluvial activity, thawing permafrost, landscape disturbance, and climatic change (Bring et al., 2016).

Despite the importance of subseasonal variations in Arctic-Boreal lakes, their temporal dynamics are poorly constrained due to a classic trade-off between high spatial versus high temporal resolution in satellite remote sensing. Most previous studies have analyzed interannual changes in lake abundance and/or area using medium-to-high resolution (~30 m) imagery (e.g., Chen et al., 2014; Jepsen et al., 2013; Jones et al., 2011; Lyons et al., 2013; Olthof et al., 2015; Plug et al., 2008; Roach et al., 2013; Smith et al., 2005; Yoshikawa & Hinzman, 2003). More recently, the now-dense Landsat archive has been used to detect seasonal to interannual trends in lake area (Nitze & Grosse, 2016; Nitze et al., 2017, 2018; Pastick et al., 2018). These studies reveal contrasting trends in lake extent variously attributed to thawing permafrost, changing water balance, hydrologic connectivity, underlying hydrogeology, shortening duration of spring snow cover, and allometric properties such as lake area. To track subseasonal changes, some studies have obtained more frequent observations using very coarse-resolution sensors (~25 km; Mialon et al., 2005; Schroeder et al., 2010; Watts et al., 2014), but these analyses cannot resolve individual lakes or lake margins. Moreover, most remote sensing studies have focused on thermokarst and/or lowland wetland terrains, notably Alaska's North Slope (e.g., Frohn et al., 2005), Yukon Flats (e.g., Chen et al., 2014), and Tuktoyaktuk Peninsula (e.g., Plug et al., 2008), whereas comparatively little research has examined much larger upland, bedrock-controlled environments in Canada. Consequently, subseasonal variability in lake area remains one of the largest uncertainties in estimates of the freshwater carbon budget (Bastviken et al., 2011; Holgerson & Raymond, 2016; Riley et al., 2011), and its drivers are poorly understood, particularly in little-studied lake-dense upland regions (Lehner & Döll, 2004; Pekel et al., 2016).

This study quantifies subseasonal dynamics in lake surface water area across four study areas in Arctic-Boreal regions of Alaska and Canada using CubeSat imagery provided by Planet Labs (Planet Team, 2018). Through deployment of hundreds of satellites in a constellation, Planet CubeSats offer both high spatial (3–5 m) and high temporal (near-daily) resolution. However, the imagery is acquired with inexpensive multispectral cameras that lack the radiometric quality, cross-sensor consistency, and geolocation accuracy of national space agency-funded missions (Cooley et al., 2017; Houborg & McCabe, 2016, 2018). To overcome these quality limitations that have, until now, prevented large-scale analyses using CubeSats, we present a novel object-based lake tracking method that incorporates machine learning. We apply this method to >75,000 CubeSat images to produce near-daily time series of surface water area for ~85,000 lakes, yielding >2.2 million individual lake observations. These observations are obtained within four strategically located study areas to capture large-scale climatic gradients, varying permafrost extent and distinctly different physiographic regions. We use this novel data set to explore the importance of permafrost presence, topography, precipitation minus evaporation, distance from rivers, mean annual air temperature, and lake allometry in controlling seasonal surface water variability. Finally, we discuss the implications of our results for freshwater inundation dynamics and carbon cycling across the Arctic-Boreal region.

2. Study Area

We track changes in lake extent across four diverse study areas spanning a range of physiographic and geological environments, namely, (1) Yukon Flats Basin (YFB), Alaska; (2) Mackenzie River Valley (MRV), Canada; (3) Canadian Shield Transect (CST), near Yellowknife, Canada; and (4) Hudson Bay Lowland (HBL), Canada. In total, these four study areas cover 226,553 km^2 of the western Arctic-Boreal region of North America (Figure 1, inset), and span Arctic tundra, boreal forest, peat plateau, lowland wetland, and upland shield terrains. The 33,383 km^2 YFB study area is characterized by fluvially disconnected wetlands surrounding a wide low-gradient reach of the Yukon River in north central Alaska (e.g., Anderson et al., 2013; Pitcher et al., 2019). The 82,200 km^2 MRV study area includes the Mackenzie River Delta, a vast, fluvially connected wetland, the Tuktoyaktuk Peninsula, a polar desert with continuous permafrost and thousands of thermokarst lakes, and boreal forest and plateaus further south along the Mackenzie and Peel Rivers (Burn & Kokelj, 2009; Plug et al., 2008). The 32,107 km^2 CST is a 350 × 90 km corridor extending from Yellowknife to the Northwest Territories-Nunavut border. It spans a lake-rich upland region consisting of exposed Precambrian bedrock surrounded by soil-filled valley bottoms (Spence & Woo, 2002, 2003, 2006). The 78,863 km^2 HBL is a 610 × 135 km transect spanning bedrock-controlled shield terrain north of Lake Winnipeg to extensive peat plateaus near the Hudson Bay coast south of Churchill, Manitoba (Wolfe et al., 2011). Taken collectively, these four study areas are broadly representative of the diverse terrains found across nonmountainous regions of Arctic-Boreal North America.

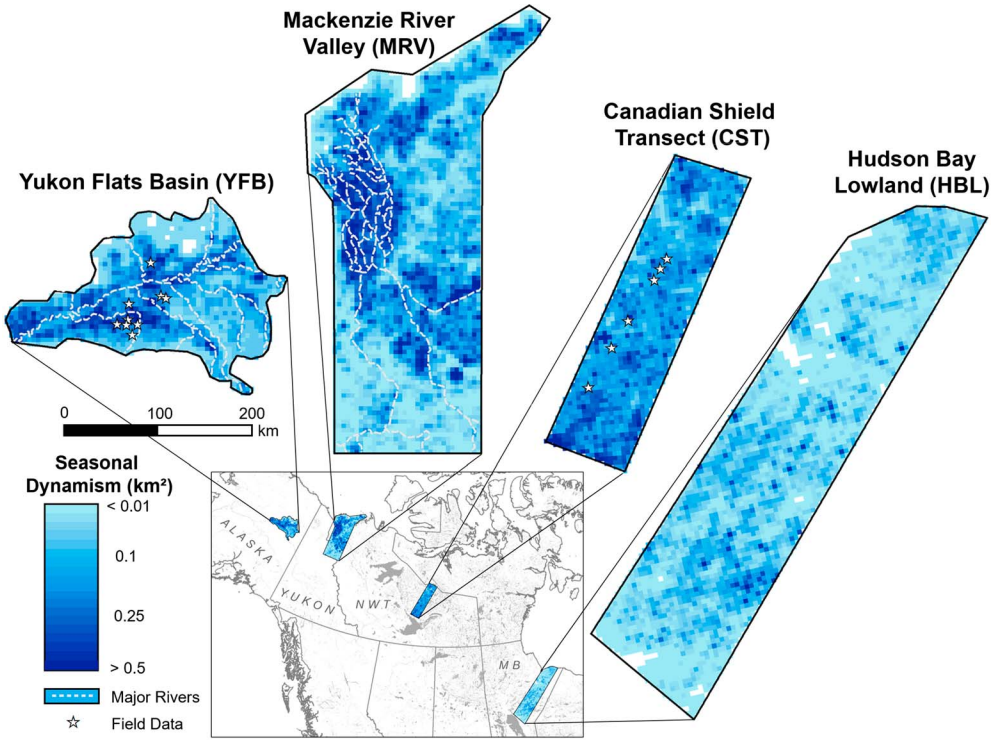

Figure 1. Gridded maps of lake dynamism (seasonal maximum minus seasonal minimum lake area, km^2) for our YFB, MRV, CST, and HBL study areas derived from CubeSat satellite imagery and machine learning. White dashed lines show major river systems (Yukon and Mackenzie Rivers and their tributaries). High dynamism is dispersed across the CST, as well as concentrated in the central YFB along the Yukon River and Mackenzie River Delta (northwest MRV). Stars indicate locations of in situ lake level measurements.

3. Methods

3.1. Data

Our primary data source is PlanetScope CubeSat satellite imagery from Planet Labs (see the supporting information; Planet Team, 2018). PlanetScope imagery has red, blue, green, and near-infrared bands with 3.125-m spatial resolution. Given its near-daily revisit time, PlanetScope accounts for 95% of all imagery analyzed. We also use RapidEye CubeSat satellite imagery from Planet Labs, which has red, blue, green, far red, and near-infrared bands at 5-m resolution and an approximate revisit time of 5 days. No cloud mask exists for either product, but Planet Labs provides a cloud index estimating the cloud-obscured fraction of each image. We analyze all imagery with less than 20% cloud obscuration and greater than 20° solar elevation angle acquired between 1 May and 1 October 2017, a collection of ~76,000 images and ~25 TB of data across our four study areas spanning the active Arctic-Boreal hydrological season.

3.2. Water Classification and Lake Tracking Method

CubeSat imagery remains underused within academic research largely due to its lack of automated cloud mask and atmospheric correction, inconsistency in cross-sensor radiometric calibration, and geolocation error (Cooley et al., 2017). To overcome these issues, we develop a novel method that incorporates object-based lake tracking and machine learning-derived observation filtering. This method is similar to that described in Cooley et al. (2017) but adapted for automation across large spatial scales. Full details of the method are described in the supporting information, and the main steps are summarized here.

The first step entails creation of a buffered lake mask used both to seed the water classification algorithm and to track changes in lake area. This mask is built through a multistep process involving initial water classification of early-season, cloud-free images, which are summed and buffered by 60 m to produce a conservative lake mask containing both the maximum seasonal extent of lakes and the surrounding land (see the

supporting information). To prevent double-counting of lake area changes, lakes whose 60-m buffer zones overlap are considered to be a singular water body for lake tracking (see the supporting information). We classify pixels as either land or water based on Normalized Difference Water Index (McFeeters, 1996) thresholds, chosen for each image based on the shape of the buffered lake mask Normalized Difference Water Index histogram (see the supporting information; Cooley et al., 2017).

Next, to track seasonal changes in lake area, we calculate the total water area contained within each lake object in the 60 m-buffered lake mask, recording an individual observation for each lake for every image (Cooley et al., 2017). This object-based lake tracking method is necessary because CubeSat imagery has a 10-m geolocation uncertainty (Cooley et al., 2017). By allowing lake boundaries to change over time, this tracking method minimizes the impact of geolocation inaccuracy on reported patterns in lake area and allows efficient change detection over our >2.2 million lake observations.

Finally, since the raw time series of lake areas include many erroneous data points caused by clouds, ice cover, or poor classification performance on images with a low signal-to-noise ratio, we use a supervised machine learning algorithm to flag poor individual lake area retrievals. For each study area, we create a manually validated training data set and use it to seed a random forests classifier (Breiman, 2001), which categorizes all lake observations as valid/invalid based on 14 predictor variables (see the supporting information). The best valid lake observation per day, defined as closest to the 5-day median, is then selected, and a 10-day median filter is applied to produce the final lake area time series. Through our observation filtering process, lakes only receive valid observations once they are ice-free, and therefore, the start dates of the lake area time series vary between early May and late June (see Figure S5).

To facilitate comparison between lake area time series, we produce a daily time series for all lakes >0.01 km^2 by interpolating between near-daily satellite observations. From the lake area time series, we calculate each lake's hydrological "dynamism," defined here as its seasonal maximum area minus seasonal minimum lake area (km^2), and percent dynamism, defined as dynamism divided by seasonal maximum lake area (%, km^2/km^2). For visualization and analysis of spatial patterns, we also sum lake dynamism to a 5 × 5 km grid for each study area (see the supporting information).

3.3. Validation and Error Analysis

We assess the accuracy of our method through both bootstrapping analyses of the manual training data and comparison with in situ pressure transducer water level measurements we collected in 15 lakes during summer 2017 (see Figures S6 and S7). The bootstrapping analysis of our observation filtering process yields RMSEs of 1,248–3,904 m^2 for mean lake area, 2,997–15,409 m^2 for maximum area, 973–22,978 m^2 for minimum area, and 5,660–23,135 m^2 for seasonal dynamism (see Table S1). As lake area is typically highly correlated with lake level, we also compare the lake area time series to our 15 in situ water level records collected in the YFB and CST. Thirteen of 15 CubeSat lake area time series are significantly correlated with water level at $p < 0.05$, with 12 correlated at $p < 0.01$, and all 15 lakes experience seasonal declines in both water level and lake area (see Figures S6–S7). While a small sample size, these simultaneous in situ measurements confirm that our remotely sensed lake area changes are both real and accurate. Furthermore, this result suggests that the dominant source of area change is lake level decline rather than vegetation growth along lake margins (see the supporting information).

3.4. Allometric and Environmental Controls on Lake Area Changes

A key challenge of interpreting temporal and spatial patterns in lake extent is the strong relationship between lake size, seasonal dynamism, and percent dynamism. Dynamism is positively correlated to lake size whereas percent change is negatively correlated to lake size (see the supporting information). To control for this effect, we develop a new lake metric, termed R_Δ, which represents the mean lateral distance (in meters) between each lake's maximum and minimum observed shoreline boundaries (see Figure S11). Because R_Δ is independent of lake area, this metric facilitates comparison of spatial patterns in surface water seasonality across different lake sizes.

Finally, we use generalized multivariable regression to analyze drivers of seasonal dynamism. We calculate gridded lake allometric variables, namely, water fraction (Figure S8), perimeter (Figure S9), number of lakes, and mean lake area from our lake area time series. We also test distance from river network, permafrost state

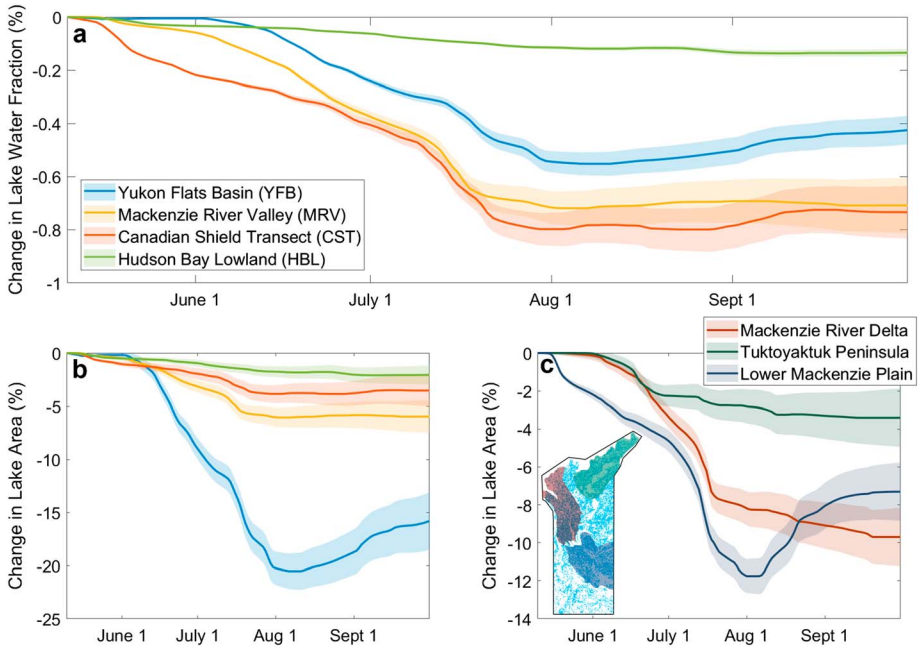

Figure 2. Temporal progression of area changes in 85,358 lakes summed across the YFB, MRV, CST, and HBL study areas calculated from >2.2 million CubeSat observations of lake area. Shaded areas are uncertainty bounds determined from RMSE values. Summed lake area changes are shown as both (a) percent of total study area (33,383, 82,200, 32,107, and 78,863 km^2, respectively), and (b) percent of maximum observed lake area (952, 9,845, 6,723, and 5,217 km^2, respectively). While YFB lakes are highly variable (blue line in b), the CST is most dynamic at the landscape scale (red line in a). Panel (c) splits the MRV (yellow line in b) into three subregions, revealing contrasting subseasonal progressions between relatively stable lakes of Tuktoyaktuk Peninsula (dark green), dynamic lakes of the fluvial-deltaic Mackenzie River Delta (maroon), and subseasonal phenological cycles in aquatic vegetation in lakes of the Lower Mackenzie Plain (navy blue).

(Brown et al., 2002), mean annual air temperature (GISTEMP Team, 2018), and precipitation minus evaporation (P – E; Figure S10; Vimal et al., 2018) and mean elevation and topographic roughness (Yamazaki et al., 2017). All variables are summed or averaged to a 5 × 5 km grid, and regressions are performed using each grid cell as an individual data point (see the supporting information).

4. Results

We identify 85,358 lakes (> 0.01 km^2) across our four study areas, with 8,854 in the YFB, 37,957 in the MRV, 21,560 in the CST, and 16,987 in the HBL. Lake size approximately follows a Pareto distribution, similar to previous lake mapping estimates (Downing et al., 2006; Lehner & Döll, 2004; Verpoorter et al., 2014). The mean lake size within each of the four study areas ranges from 0.11 (±0.25) km^2 (YFB) to 0.31 (±1.82) km^2 (CST) with an average value of 0.26 (±1.45) km^2 across all four. Over the course of the study period, the mean total lake areas are 802 (YFB), 9,336 (MRV), 6,479 (CST), and 5,082 (HBL) km^2. Converted to units of water fraction (lake surface area divided by total study area), the highest water fraction is found on the CST (20.2%), followed by the MRV (11.4%), HBL (6.4%), and YFB (2.4%).

On average, Arctic-Boreal lakes receive a valid, cloud-free observation once every 5.2 (±1.9) days, varying from 4.1 (±1.0) for the YFB to 6.2 (±1.8) for the MRV. We find a near-universal decline in lake extent during the study period, which is widespread across all four study areas, including lowland wetland and upland bedrock terrains (Figure 1). These declines are consistent with in situ observations of water level (Figures S6 and S7) and reflect broadly negative summer P − E over Northern North America in 2017 (Figure S10). The YFB, MRV, and CST show remarkable similarity in their subseasonal progression, decreasing steeply from the start of the open water season until the end of July and then remaining mostly stable or increasing slightly through the end of September (Figure 2). In contrast, the HBL declines gradually and is more stable overall, perhaps due to its lack of well-developed river networks, low water fraction, and high water storage in its peatland terrain (Smith et al., 2012; Figure 2).

Gridded maps of lake dynamism reveal loci of spring flooding in the YFB and MRD as well as substantial, dispersed dynamism throughout the CST (Figure 1). The percent dynamism is 29% (dynamism = 279 km^2) for YFB, 9% (907 km^2) for MRV, 7% (439 km^2) for CST, and 5% (247 km^2) for HBL (Figure 2b). The mean individual lake percent change is comparable for the MRV, CST, and HBL (17%, 18%, and 15%), but higher in the YFB where, on average, lakes change by 39%. However, when lake dynamism is considered at the landscape scale, the change in surface water extent per unit land area is 0.8%, 1.1%, 1.4%, and 0.3%, for the four study areas, respectively. In other words, the greatest change in lake water fraction is found in the CST, where 1.4% of the total landscape is seasonally inundated, nearly double that of the YFB.

The high spatial resolution and dense temporal sampling afforded by CubeSats also reveal distinct localized exceptions to the broader seasonal decline, as exemplified by local concentrations of lake dynamism within the MRV (Figure 2c). The Mackenzie River Delta undergoes a steep decline (~8%) in lake area until mid-July, after which lake areas stabilize, a progression likely associated with floodplain inundation following ice breakup and peak river discharge. In contrast, the thermokarst-dominated Tuktoyaktuk Peninsula experiences a small, gradual seasonal decline (~3%) in total lake area, and the Lower Mackenzie Plain declines sharply through July (~12%) before rebounding in August and September (Figure 2c). Visual inspection reveals that this distinct signal in the Lower Mackenzie Plain is primarily driven by a high incidence of lakes that experience a large change in area due to rapid emergence and then decline of aquatic vegetation and/or algae at their surface. When mapped across the four study areas, we find these "vegetation-impacted" lakes account for 1–2% of all lakes studied and 7–13% of the observed dynamism across the YFB, MRV, and CST, with particular concentration in the Lower Mackenzie Plain and the southern tip of the CST (see Figure S12).

CubeSat observations of R_Δ (i.e., mean lateral distance between maximum and minimum lake boundaries) reveal that most Arctic-Boreal lake dynamism is driven by small shoreline fluctuations of ≤10 m (Figure 3). Across all study areas, the mean R_Δ is 6.6 (±8.6) m, varying from 5.0 (±5.0) m in the HBL to 13.0 (±13.0) m in the YFB. Large R_Δ values are primarily associated with floodplains and vegetation-impacted lakes, whereas low R_Δ values predominate in upland regions (Figure 3). For the YFB, lakes with a $R_\Delta \leq 10$ m account for just 28% of the observed dynamism, whereas they account for 54% in the MRV and 76% in both the CST and HBL. This suggests that landscape-scale lake dynamism is dominated by fewer highly dynamic lakes in the YFB versus many comparatively stable lakes in the CST and HBL, with the CST displaying the greatest overall dynamism due to the cumulative small shoreline fluctuations of many more lakes (Figure 2a; white asterisk in Figure 3).

Multivariable regression of gridded lake dynamism with allometric (water fraction, lake perimeter, number of lakes, and mean lake size) and environmental (elevation, topographic roughness, permafrost presence, mean annual air temperature, distance to river, and P − E) variables indicates that total seasonal dynamism strongly depends on lake allometry. The regression models built using these 10 variables explain 74%, 65%, 58%, and 55% of the total variance in seasonal dynamism for the four study areas, respectively (Figure S13; Table S2). Between 87% (CST) and 99% (YFB and MRV) of the explanatory power is associated with perimeter and water fraction alone. In contrast, environmental variables explain only 2–16% of the observed dynamism, with permafrost and mean annual air temperature the strongest predictors, suggesting little detectable environmental control on lake dynamism over the study period (see the supporting information).

5. Discussion

Our object-based CubeSat lake tracking method allows us to monitor fine-scale changes in surface water with high temporal frequency across large spatial scales. The combination of 3- to 5-m spatial resolution and ~5-day average cloud-free revisit time yielded >2.2 million observations of lakes as small as 0.01 km^2 in just 5 months. By using machine learning to filter out low-quality observations, some critical limitations of CubeSat imagery are overcome, enabling scientific analysis of thousands of images and millions of individual lake observations. Consequently, our analysis of ~85,000 lakes reveals both broad-scale similarities and novel fine-scale anomalies in subseasonal inundation dynamics of Arctic-Boreal lakes.

Broadly, we observe a universal, synchronous seasonal drawdown in surface water extent across our four study areas throughout the 2017 open-water season. This finding differs from most studies of surface

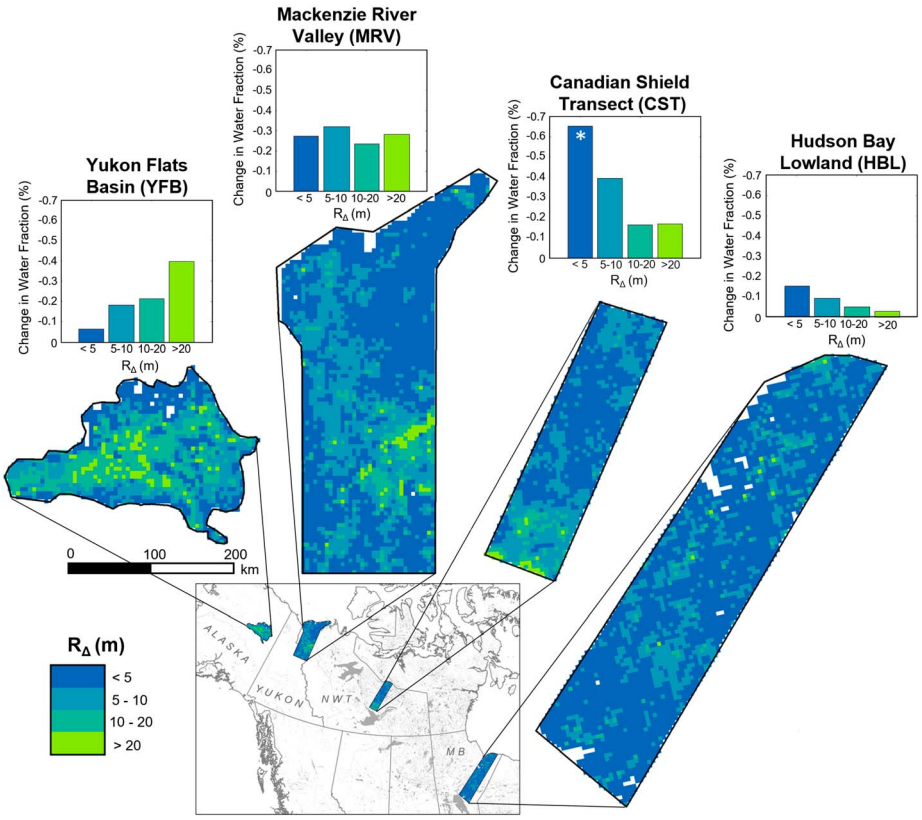

Figure 3. Gridded maps of mean lateral distance between maximum and minimum observed lake boundaries (R_Δ, m) for YFB, MRV, CST, and HBL. Bar graphs quantify the change in lake water fraction (%) associated with lakes within specified R_Δ ranges. The CST displays the highest overall change in lake water fraction, dominated especially by small shoreline fluctuations ($R_\Delta \leq 5$, white asterisk).

water dynamics in Arctic-Boreal regions, which tend to focus on dynamic, flood-prone lowlands such as the Yukon Flats (Anderson et al., 2013; Chen et al., 2014; Jepsen et al., 2016), Mackenzie River Delta (Goulding et al., 2009; Lesack et al., 2013; Marsh & Lesack, 1996), and Peace-Athabasca Delta (Pavelsky & Smith, 2008). While our study confirms that lakes in such environments are hydrologically dynamic, it also shows that their relatively small areas and comparatively low water fractions may make them less important to continental-scale surface water variability than the outsized attention they receive might suggest. Indeed, in absolute terms we identify more *total* lake dynamism elsewhere. Lake percent area changes and R_Δ values are lower in upland regions like the CST and southeastern HBL, likely due to higher topographic variability and poorly developed fluvial drainage. However, when multiplied across large, lake-rich areas, these small shoreline changes cumulatively produce large absolute changes in lake surface area across the landscape.

This effect is exemplified by the contrast between the CST and the heavily studied YFB, which are similar in size (32,107 and 33,383 km^2) yet display vastly different subseasonal dynamics in lake area. Despite containing few highly dynamic lakes and a smaller percent dynamism (7% vs. 29%), the CST experiences significantly more *absolute* lake dynamism than the YFB (439 km^2 vs. 279 km^2) due to its much larger water fraction (20% vs. 2%). Previous surface water studies have largely ignored this landscape-scale effect. Coarse-resolution global/pan-Arctic analyses do include the Canadian Shield but have difficulty resolving the fine-scale changes that dominate subseasonal lake dynamics in this area. For example, a comparison of our CubeSat results with a recent global Landsat-based seasonality product (Pekel et al., 2016) finds that even the 30 m, ~16-day revisit time of this high-quality product likely underestimates total seasonal dynamism by up to 50% (Figure S14), especially in the CST, where small shoreline fluctuations (low R_Δs) dominate. While some of this difference may be due to interannual variability (see the supporting information), this improved quantification of lake dynamism in the CST is likely an outcome of the high spatial resolution

of CubeSat imagery, which enables mapping of numerous small, previously undetectable lake shoreline changes that sum to large areas of intermittently inundated land.

Our quantification of substantial, widespread dynamism accrued from small shoreline fluctuations of many lakes is consequential for estimates of trace gas emissions from freshwater bodies. In contrast to the relatively "static" view of upland lakes commonly assumed by CH_4 and CO_2 emission models (Bastviken et al., 2011; Matthews & Fung, 1987; Raymond et al., 2013; Ringeval et al., 2010; Watts et al., 2014), our results suggest that all Arctic-Boreal landscapes are dynamic and often at fine spatial scales missed by coarse-resolution products. This finding is inherently conservative, as we consider only open-water lake shorelines in this study, whereas Arctic-Boreal lake fluctuations commonly recharge surrounding wetlands as well. Furthermore, littoral, seasonally inundated shorelines and wetlands are known "hotspots" of freshwater CO_2 and CH_4 production and emission (Bastviken et al., 2004; Tranvik et al., 2009), suggesting that 1 km^2 of intermittently inundated land comprised of numerous small shoreline fluctuations likely emits more trace gas than 1 km^2 of permanently inundated land owing to shallow water, vegetation, and CO_2 supersaturation. Lastly, because Shield landscapes have both high water fractions and high lake densities, they typically have a very high lake perimeter to land surface area ratio (2.3 km/km^2 for CST vs. 0.6 km/km^2 for YFB), and thus, the total area of intermittently inundated lake shorelines potentially contributing to CO_2 emission in upland regions is large.

Finally, our analysis of potential drivers of subseasonal surface water dynamism identifies an outsized importance of lake allometry (Lyons et al., 2013; Smith & Pavelsky, 2009), and particularly lake perimeter, on spatiotemporal patterns in lake area change. Other variables commonly cited as drivers of interannual lake surface area change, such as water balance (Anderson et al., 2013; Chen et al., 2014; Plug et al., 2008; Riordan et al., 2006), permafrost presence (Jepsen et al., 2013; Smith et al., 2005; Walvoord et al., 2012), and distance from river networks (Roach et al., 2013), appear to have a negligible effect on intra-annual lake dynamism compared to lake allometry. Better ancillary data sets could produce different results, and we suggest future work to confirm or refute this finding, but a clear conclusion of our study is that any broad-scale study seeking to attribute lake area changes to permafrost, climate, or other external factors must first control for lake allometry. Given that these factors influence lake allometry themselves (Smith et al., 2007), future work should also consider the interactions between lake allometry and environmental variables.

6. Conclusion

Our Arctic-Boreal lake tracking analysis advances the utility of CubeSat imagery for hydrologic research. At the local scale, the high temporal and spatial resolutions of CubeSat imagery reveal short-lived phenomena such as floodplain inundation and aquatic vegetation phenology, observations that can inform a wide range of applications including carbon cycling (Bastviken et al., 2004; Tranvik et al., 2009), water quality (Palmer et al., 2015), and hydrologic connectivity (Pavelsky & Smith, 2008). At the broad scale, we identify a ubiquitous drawdown of surface water across northern North America during summer 2017, including substantial water loss caused by fine-scale lake shoreline contractions on the lake-dense Canadian Shield, which coarser-resolution sensors miss. This finding suggests that current models of CO_2 and CH_4 trace gas emission from inland waters underestimate the importance of subseasonal lake area dynamics.

Acknowledgments
This research was funded by the NASA Terrestrial Ecology Program Arctic-Boreal Vulnerability Experiment (ABoVE) Grant NNX17AC60A. S. Cooley is also funded by a National Science Foundation Graduate Research Fellowship. We thank Planet Labs Education and Research Program Director Joseph Mascaro and the Planet Labs Ambassador Program for providing access to all PlanetScope and RapidEye imagery. We thank David Butman (University of Washington), Simon Topp (University of North Carolina at Chapel Hill), and Mark Bertram and Heather Bartlett (Yukon Flats National Wildlife Refuge) for their assistance in collecting in situ lake level records in the Yukon Flats Basin. We thank the Gwichyaa Zhee Gwich'in Tribal Government and Doyon Limited along with the Yukon Flats National Wildlife Refuge and the U.S. Fish and Wildlife Service for access to the lands and waterways of the Yukon Flats. We thank Bruce Hanna (Government of the Northwest Territories Environment and Natural Resource Division) and Dave Olesen for their assistance in collecting lake level records in the Canadian Shield Transect. Finally, we thank Henry Johnson (Brown University) for support with computing and data storage. The CubeSat-derived lake area time series and associated metadata are archived at the Oak Ridge National Laboratory Distributed Active Archive Center (ORNL DAAC) and can be accessed here: https://doi.org/10.3334/ORNLDAAC/1667. We thank Ben Jones and an anonymous reviewer for their insightful feedback on an earlier version of this manuscript.

References

Anderson, L., Birks, J., Rover, J., & Guldager, N. (2013). Controls on recent Alaskan lake changes identified from water isotopes and remote sensing. *Geophysical Research Letters*, *40*, 3413–3418. https://doi.org/10.1002/grl.50672

Bastviken, D., Cole, J., Pace, M., & Tranvik, L. (2004). Methane emissions from lakes: Dependence of lake characteristics, two regional assessments, and a global estimate. *Global Biogeochemical Cycles*, *18*, GB4009. https://doi.org/10.1029/2004GB002238

Bastviken, D., Tranvik, L. J., Downing, J. A., Crill, P. M., & Enrich-Prast, A. (2011). Freshwater methane emissions offset the continental carbon sink. *Science*, *331*(6013), 50. https://doi.org/10.1126/science.1196808

Breiman, L. (2001). Random forests. *Machine Learning*, *45*(1), 5–32. https://doi.org/10.1023/A:1010933404324

Bring, A., Fedorova, I., Dibike, Y., Hinzman, L., Mård, J., Mernild, S. H., Prowse, T., et al. (2016). Arctic terrestrial hydrology: A synthesis of processes, regional effects, and research challenges. *Journal of Geophysical Research: Biogeosciences*, *121*, 621–649. https://doi.org/10.1002/2015JG003131

Brown, J., Ferrians, J., Heginbottom, A., & Melnikov, E. (2002). Circum-Arctic map of permafrost and ground-ice conditions, version 2. Boulder, CO: NSIDC: National Snow and Ice Data Center.

Burn, C. R., & Kokelj, S. V. (2009). The environment and permafrost the Mackenzie Delta area. *Permafrost and Periglacial Processes*, *20*(2), 83–105. https://doi.org/10.1002/ppp.655

Chen, M., Rowland, J. C., Wilson, C. J., Altmann, G. L., & Brumby, S. P. (2014). Temporal and spatial pattern of thermokarst lake area changes at Yukon Flats, Alaska. *Hydrological Processes*, *28*(3), 837–852. https://doi.org/10.1002/hyp.9642

Cooley, S. W., Smith, L. C., Stepan, L., & Mascaro, J. (2017). Tracking dynamic northern surface water changes with high-frequency planet CubeSat imagery. *Remote Sensing*, *9*(12), 1–21. https://doi.org/10.3390/rs9121306

Downing, J. A., Prairie, Y. T., Cole, J. J., Duarte, C. M., Tranvik, L. J., Striegl, R. G., et al. (2006). The global abundance and size distribution of lakes, ponds, and impoundments. *Limnology and Oceanography*, *51*(5), 2388–2397. https://doi.org/10.1016/B978-012370626-3.00025-9

Frohn, R. C., Hinkel, K. M., & Eisner, W. R. (2005). Satellite remote sensing classification of thaw lakes and drained thaw lake basins on the North Slope of Alaska. *Remote Sensing of Environment*, *97*, 116–126. https://doi.org/10.1016/j.rse.2005.04.022

GISTEMP Team. (2018). *GISS surface temperature analysis (GISTEMP)*. NASA Goddard Institute for Space Studies.

Goulding, H. L., Prowse, T. D., & Beltaos, S. (2009). Spatial and temporal patterns of break-up and ice-jam flooding in the Mackenzie Delta, NWT. *Hydrological Processes*, *23*(18), 2654–2670. https://doi.org/10.1002/hyp.7251

Hastie, A., Lauerwald, R., Weyhenmeyer, G., Sobek, S., Verpoorter, C., & Regnier, P. (2018). CO_2 evasion from boreal lakes: Revised estimate, drivers of spatial variability, and future projections. *Global Change Biology*, *24*(2), 711–728.

Holgerson, M. A., & Raymond, P. A. (2016). Large contribution to inland water CO2 and CH4 emissions from very small ponds. *Nature Geoscience*, *9*(3), 222–226. https://doi.org/10.1038/ngeo2654

Houborg, R., & McCabe, M. F. (2016). High-resolution NDVI from planet's constellation of earth observing nano-satellites: A new data source for precision agriculture. *Remote Sensing*, *8*(9). https://doi.org/10.3390/rs8090768

Houborg, R., & McCabe, M. F. (2018). A Cubesat enabled spatio-temporal enhancement method (CESTEM) utilizing Planet, Landsat and MODIS data. *Remote Sensing of Environment*, *209*, 211–226. https://doi.org/10.1016/j.rse.2018.02.067

Jepsen, S. M., Voss, C. I., Walvoord, M. A., Rose, J. R., Minsley, B. J., & Smith, B. D. (2013). Sensitivity analysis of lake mass balance in discontinuous permafrost: The example of disappearing Twelvemile Lake, Yukon Flats, Alaska (USA). *Hydrogeology Journal*, *21*(1), 185–200. https://doi.org/10.1007/s10040-012-0896-5

Jepsen, S. M., Walvoord, M. A., Voss, C. I., & Rover, J. (2016). Effect of permafrost thaw on the dynamics of lakes recharged by ice-jam floods: Case study of Yukon Flats, Alaska. *Hydrological Processes*, *30*(11), 1782–1795. https://doi.org/10.1002/hyp.10756

Jones, B. M., Grosse, G., Arp, C. D., Jones, M. C., Walter Anthony, K. M., & Romanovsky, V. E. (2011). Modern thermokarst lake dynamics in the continuous permafrost zone, northern Seward Peninsula, Alaska. *Journal of Geophysical Research*, *116*, G00M03. https://doi.org/10.1029/2011JG001666

Kirschke, S., Bousquet, P., Ciais, P., Saunois, M., Canadell, J. G., Dlugokencky, E. J., Bergamaschi, P., et al. (2013). Three decades of global methane sources and sinks. *Nature Geoscience*, *6*(10), 813–823. https://doi.org/10.1038/ngeo1955

Lehner, B., & Döll, P. (2004). Development and validation of a global database of lakes, reservoirs and wetlands. *Journal of Hydrology*, *296*(1–4), 1–22. https://doi.org/10.1016/j.jhydrol.2004.03.028

Lesack, L. F. W., Marsh, P., Hicks, F. E., & Forbes, D. L. (2013). Timing, duration, and magnitude of peak annual water-levels during ice breakup in the Mackenzie Delta and the role of river discharge. *Water Resources Research*, *49*, 8234–8249. https://doi.org/10.1002/2012WR013198

Lyons, S. R., Sheng, Y., Smith, L. C., Li, J., Hinkel, K. M., Lenters, J. D., & Wang, J. (2013). Quantifying sources of error in multitemporal multisensor lake mapping. *International Journal of Remote Sensing*, *23*(22), 7887–7905. https://doi.org/10.1080/01431161.2013.8273432013

Marsh, P., & Lesack, L. F. W. (1996). The hydrologic regime of perched lakes in the Mackenzie Delta: Potential responses to climate change. *Limnology and Oceanography*, *41*(5), 849–856. https://doi.org/10.4319/lo.1996.41.5.0849

Matthews, E., & Fung, I. (1987). Methane emission from natural wetlands: Global distribution, area, and environmental characteristics of sources. *Global Biogeochemical Cycles*, *1*(1), 61–86. https://doi.org/10.1029/GB001i001p00061

McFeeters, S. K. (1996). The use of the Normalized Difference Water Index (NDWI) in the delineation of open water features. *International Journal of Remote Sensing*, *17*(7), 1425–1432. https://doi.org/10.1080/01431169608948714

Mialon, A., Royer, A., & Fily, M. (2005). Wetland seasonal dynamics and interannual variability over northern high latitudes, derived from microwave satellite data. *Journal of Geophysical Research*, *110*, D17102. https://doi.org/10.1029/2004JD005697

Nitze, I., & Grosse, G. (2016). Detection of landscape dynamics in the Arctic Lena Delta with temporally dense Landsat time-series stacks. *Remote Sensing of Environment*, *181*, 27–41. https://doi.org/10.1016/j.rse.2016.03.038

Nitze, I., Grosse, G., Jones, B. M., Arp, C. D., Ulrich, M., Fedorov, A., & Veremeeva, A. (2017). Landsat-based trend analysis of lake dynamics across northern permafrost regions. *Remote Sensing*, *9*(7), 1–28. https://doi.org/10.3390/rs9070640

Nitze, I., Grosse, G., Jones, B. M., Romanovsky, V. E., & Boike, J. (2018). Remote sensing quantifies widespread abundance of permafrost region disturbances across the Arctic and Subarctic. *Nature Communications*, *9*(1), 5423. https://doi.org/10.1038/s41467-018-07663-3

Olthof, I., Fraser, R. H., & Schmitt, C. (2015). Landsat-based mapping of thermokarst lake dynamics on the Tuktoyaktuk Coastal Plain, Northwest Territories, Canada since 1985. *Remote Sensing of Environment*, *168*, 194–204. https://doi.org/10.1016/j.rse.2015.07.001

Palmer, S. C. J., Kutser, T., & Hunter, P. D. (2015). Remote sensing of inland waters: Challenges, progress and future directions. *Remote Sensing of Environment*, *157*, 1–8. https://doi.org/10.1016/j.rse.2014.09.021

Pastick, N. J., Jorgenson, M. T., Goetz, S. J., Jones, B. M., Wylie, B. K., Minsley, B. J., Genet, H., et al. (2018). Spatiotemporal remote sensing of ecosystem change and causation across Alaska. *Global Change Biology*. https://doi.org/10.1111/gcb.14279

Pavelsky, T. M., & Smith, L. C. (2008). Remote sensing of hydrologic recharge in the peace-Athabasca Delta, Canada. *Geophysical Research Letters*, *35*, L08403. https://doi.org/10.1029/2008GL033268

Pekel, J.-F., Cottam, A., Gorelick, N., & Belward, A. S. (2016). High-resolution mapping of global surface water and its long-term changes. *Nature*, *540*(7633), 418–422. https://doi.org/10.1038/nature20584

Pitcher, L. H., Pavelsky, T. M., Smith, L. C., Moller, D. K., Altenau, E. H., Allen, G. H., et al. (2019). AirSWOT InSAR mapping of surface water elevations and hydraulic gradients across the Yukon Flats Basin, Alaska. *Water Resources Research*. https://doi.org/10.1029/2018WR023274

Planet Team. (2018). Planet application program interface: In space for life on Earth. San Francisco, CA. Retrieved from https://api.planet.com

Plug, L. J., Walls, C., & Scott, B. M. (2008). Tundra lake changes from 1978 to 2001 on the Tuktoyaktuk Peninsula, western Canadian Arctic. *Geophysical Research Letters*, *35*, L03502. https://doi.org/10.1029/2007GL032303

Raymond, P. A., Hartmann, J., Lauerwald, R., Sobek, S., McDonald, C., Hoover, M., Butman, D., et al. (2013). Global carbon dioxide emissions from inland waters. *Nature*, *503*(7476), 355–359. https://doi.org/10.1038/nature12760

Riley, W. J., Subin, Z. M., Lawrence, D. M., Swenson, S. C., Torn, M. S., Meng, L., Mahowald, N. M., et al. (2011). Barriers to predicting changes in global terrestrial methane fluxes: Analyses using CLM4Me, a methane biogeochemistry model integrated in CESM. *Biogeosciences*, *8*(7), 1925–1953. https://doi.org/10.5194/bg-8-1925-2011

Ringeval, B., De Noblet-Ducoudré, N., Ciais, P., Bousquet, P., Prigent, C., Papa, F., & Rossow, W. B. (2010). An attempt to quantify the impact of changes in wetland extent on methane emissions on the seasonal and interannual time scales. *Global Biogeochemical Cycles*, *24*, GB2003. https://doi.org/10.1029/2008GB003354

Riordan, B., Verbyla, D., & McGuire, A. D. (2006). Shrinking ponds in subarctic Alaska based on 1950–2002 remotely sensed images. *Journal of Geophysical Research*, *111*, G04002. https://doi.org/10.1029/2005JG000150

Roach, J. K., Griffith, B., & Verbyla, D. (2013). Landscape influences on climate-related lake shrinkage at high latitudes. *Global Change Biology*, *19*(7), 2276–2284. https://doi.org/10.1111/gcb.12196

Schroeder, R., Rawlins, M. A., McDonald, K. C., Podest, E., Zimmermann, R., & Kueppers, M. (2010). Satellite microwave remote sensing of North Eurasian inundation dynamics: Development of coarse-resolution products and comparison with high-resolution synthetic aperture radar data. *Environmental Research Letters*, *5*(1), 015003. https://doi.org/10.1088/1748-9326/5/1/015003

Smith, L. C., Beilman, D. W., Kremenetski, K. V., Sheng, Y., MacDonald, G. M., Lammers, R. B., Shiklomanov, A. I., et al. (2012). Influence of permafrost on water storage in West Siberian peatlands revealed from a new database of soil properties. *Permafrost and Periglacial Processes*, *23*(1), 69–79. https://doi.org/10.1002/ppp.735

Smith, L. C., & Pavelsky, T. M. (2009). Remote sensing of volumetric storage changes in lakes. *Earth Surface Processes and Landforms*, *34*, 1343–1358. https://doi.org/10.1002/esp.1822

Smith, L. C., Sheng, Y., & MacDonald, G. M. (2007). A first pan-Arctic assessment of the influence of glaciation, permafrost, topography and peatlands on Northern Hemisphere lake distribution. *Permafrost and Periglacial Processes*, *20*, 173–184. https://doi.org/10.1002/ppp.581

Smith, L. C., Sheng, Y., MacDonald, G. M., & Hinzman, L. D. (2005). Disappearing Arctic lakes. *Science*, *308*, 1429. https://doi.org/10.1126/science.1108142

Spence, C., & Woo, M. K. (2002). Hydrology of subarctic Canadian shield: Bedrock upland. *Journal of Hydrology*, *262*(1–4), 111–127. https://doi.org/10.1016/S0022-1694(02)00010-0

Spence, C., & Woo, M. K. (2003). Hydrology of subarctic Canadian shield: Soil-filled valleys. *Journal of Hydrology*, *279*(1–4), 151–166. https://doi.org/10.1016/S0022-1694(03)00175-6

Spence, C., & Woo, M. K. (2006). Hydrology of subarctic Canadian shield: Heterogeneous headwater basins. *Journal of Hydrology*, *317*(1–2), 138–154. https://doi.org/10.1016/j.jhydrol.2005.05.014

Stackpoole, S. M., Butman, D. E., Clow, D. W., Verdin, K. L., Gaglioti, B. V., Genet, H., & Striegl, R. G. (2017). Inland waters and their role in the carbon cycle of Alaska. *Ecological Applications*, *27*(5), 1403–1420. https://doi.org/10.1002/eap.1552

Tranvik, L. J., Downing, J. A., Cotner, J. B., Loiselle, S. A., Striegl, R. G., Ballatore, T. J., Dillon, P., et al. (2009). Lakes and reservoirs as regulators of carbon cycling and climate. *Limnology and Oceanography*, *54*(6part2), 2298–2314. https://doi.org/10.4319/lo.2009.54.6_part_2.2298

Verpoorter, C., Kutser, T., Seekell, D. A., & Tranvik, L. J. (2014). A global inventory of lakes based on high-resolution satellite imagery. *Geophysical Research Letters*, *41*, 6396–6402. https://doi.org/10.1002/2014GL060641

Vimal, S., Lettenmaier, D. P., & Smith, L. C. (2018). Hydrological fluxes from 1979–2018 for Canada and Alaska. Oak Ridge National Laboratory (ORNL) Distributed Active Archive Center (DAAC) for biogeochemical dynamics.

Walvoord, M. A., Voss, C. I., & Wellman, T. P. (2012). Influence of permafrost distribution on groundwater flow in the context of climate-driven permafrost thaw: Example from Yukon Flats Basin, Alaska, United States. *Water Resources Research*, *48*, W07524. https://doi.org/10.1029/2011WR011595

Watts, J. D., Kimball, J. S., Bartsch, A., & McDonald, K. C. (2014). Surface water inundation in the boreal-Arctic: Potential impacts on regional methane emissions. *Environmental Research Letters*, *9*(7). https://doi.org/10.1088/1748-9326/9/7/075001

Wolfe, B. B., Light, E. M., Macrae, M. L., Hall, R. I., Eichel, K., Jasechko, S., White, J., et al. (2011). Divergent hydrological responses to 20th century climate change in shallow tundra ponds, western Hudson Bay Lowlands. *Geophysical Research Letters*, *38*, L23402. https://doi.org/10.1029/2011GL049766

Yamazaki, D., Ikeshima, D., Tawatari, R., Yamaguchi, T., O'Loughlin, F., Neal, J. C., Sampson, C. C., et al. (2017). A high-accuracy map of global terrain elevations. *Geophysical Research Letters*, *44*, 5844–5853. https://doi.org/10.1002/2017GL072874

Yoshikawa, K., & Hinzman, L. D. (2003). Shrinking thermokarst ponds and groundwater dynamics in discontinuous permafrost near Council, Alaska. *Permafrost and Periglacial Processes*, *14*(2), 151–160. https://doi.org/10.1002/ppp.451